

Strangeness in Nuclear Collisions

Marek Gaździcki¹ and Dieter Röhrich²

Abstract

Data on the mean multiplicity of strange hadrons produced in minimum bias proton–proton and central nucleus–nucleus collisions at momenta between 2.8 and 400 GeV/c per nucleon have been compiled. The multiplicities for nucleon–nucleon interactions were constructed. The ratios of strange particle multiplicity to participant nucleon as well as to pion multiplicity are larger for central nucleus–nucleus collisions than for nucleon–nucleon interactions at all studied energies. The data at AGS energies suggest that the latter ratio saturates with increasing masses of the colliding nuclei. The strangeness to pion multiplicity ratio observed in nucleon–nucleon interactions increases with collision energy in the whole energy range studied. A qualitatively different behaviour is observed for central nucleus–nucleus collisions: the ratio rapidly increases when going from Dubna to AGS energies and changes little between AGS and SPS energies. This change in the behaviour can be related to the increase in the entropy production observed in central nucleus–nucleus collisions at the same energy range. The results are interpreted within a statistical approach. They are consistent with the hypothesis that the Quark Gluon Plasma is created at SPS energies, the critical collision energy being between AGS and SPS energies.

Z. Phys. **C71** (1996) 55.

October 17, 2018

¹E–mail address: marek@ikf.uni–frankfurt.de

²E–mail address: roehrich@ikf.uni–frankfurt.de

1 Introduction

The origin of quark confinement inside hadrons and the origin of masses of known particles are two distinct problems of modern physics [1]. It is expected that at high enough energy density quarks are deconfined and their masses, due to chiral symmetry restoration, are small in comparison with constituent quark masses or masses of hadrons. This new form of matter conjectured long ago [2] is called Quark Gluon Plasma [3].

Experimental studies of the Quark Gluon Plasma properties should help to understand the puzzles of quark confinement and particle masses. In such investigations high energy nuclear collisions play a unique role [4]. They allow to create ‘macroscopic’ (in comparison to the characteristic scale of strong interaction ≈ 1 fm) space–time regions with high energy density in the laboratory. Their volumes and the energy densities are controlled by the sizes of the colliding nuclei and their collision energy.

Recent data on central Pb+Pb collisions at the highest energy available in the laboratory (CERN SPS: $\sqrt{s} \approx 20$ A·GeV) indicate that matter with energy density of several GeV/fm³ is created at the early stage of the collision [5]. This estimated energy density is significantly higher than the critical energy density ($\epsilon \approx 1$ GeV/fm³) at which a transition to a Quark Gluon Plasma takes place according to recent QCD lattice simulations [6]. Thus the crucial question is: Do we create a Quark Gluon Plasma already in central nucleus–nucleus collisions at the CERN SPS? It is difficult to answer this question because analysis of the observed potential signals of a Quark Gluon Plasma creation, like strangeness enhancement [7, 8, 9] and J/Ψ suppression [10, 11] is model dependent and obscured by the problems with an exact theoretical description of high energy nucleus–nucleus collisions, in which nonperturbative QCD processes dominate the dynamics.

In order to limit uncertainties in the data interpretation we have undertaken a systematic study of the experimental results as a function of the collision energy and the mass number of the colliding nuclei. Sudden changes in the studied dependences may indicate that a critical collision energy and/or a critical volume is crossed. In fact in a previous work we showed that the particle multiplicity (entropy) rapidly increases in the energy region between $\sqrt{s} \approx 5$ A·GeV (BNL AGS) and $\sqrt{s} \approx 20$ A·GeV (CERN SPS) for large enough colliding nuclei [12, 13]. This increase can be interpreted as due to a transition to a Quark Gluon Plasma. Using a statistical approach it was estimated that this transition is connected with the increase of the effective number of degrees of freedom by a factor of about 3 [13].

In this work we compile the experimental data on strangeness production in nuclear collisions. We study their dependences on the collisions energy and the volume of the colliding systems. We attempt to interpret the results within a statistical approach. The paper is organized as follows: The experimental data on strange hadron production in nucleon–nucleon interactions and central nucleus–nucleus collisions are compiled in Sections 2 and 3. The results are discussed in Section 4 and interpreted in Section 5.

2 Nucleon–Nucleon Interactions

Data on strange particle production in nucleon–nucleon interactions are necessary as reference data in order to study strangeness production in nucleus–nucleus collisions. In this section we first compile and discuss data on multiplicity of strange hadrons produced in minimum bias p+p interactions. Using these data, in the second part of the section, we construct the strange particle multiplicities in nucleon–nucleon interactions.

2.1 Compilation of p+p Data

Data on the mean multiplicity of Λ , $\bar{\Lambda}$ hyperons, $\langle\Lambda\rangle_{pp}$, $\langle\bar{\Lambda}\rangle_{pp}$, and K_S^0 mesons, $\langle K_S^0\rangle_{pp}$, produced in minimum bias p+p interactions [14] are summarized in Table 1. The dependence of $\langle\Lambda\rangle_{pp}$, $\langle\bar{\Lambda}\rangle_{pp}$ and $\langle K_S^0\rangle_{pp}$ on the collision energy is shown in Figs. 1, 2 and 3, respectively. The multiplicities are plotted against the Fermi variable [15]:

$$F = \frac{(\sqrt{s} - 2 \cdot m_p)^{3/4}}{\sqrt{s}^{1/4}}, \quad (1)$$

where m_p is the proton rest mass and \sqrt{s} is the collision energy in the center of mass system. In Figs. 1, 2 and 3 the results obtained at 24.5 GeV/c [14] are not included because the Λ hyperon multiplicity presented there (see Table 1) is two times lower than the value expected using the systematics of all other measurements.

In this paper $\langle\Lambda\rangle$ denotes the average multiplicity of Λ hyperons produced directly (by strong interactions), originating from electromagnetic decays of Σ^0 hyperons and in addition a fraction of Λ hyperons from Ξ decays. Treatment of Λ hyperons originating from weak decays of Ξ s is usually not discussed in an explicit way in the experimental papers. The Ξ/Λ ratio is about 3% at $p_{LAB} = 19$ GeV/c and 10% at $\sqrt{s} = 63$ GeV (see Ref. [16] and references therein). From the description of the analysis procedure used in most of the experiments follows that the Λ hyperons from Ξ decays are (at least in part) included in the published $\langle\Lambda\rangle$ multiplicity. The same argument applies to the $\bar{\Lambda}$ multiplicity.

The data on mean multiplicities of K^+ , $\langle K^+\rangle_{pp}$, and K^- , $\langle K^-\rangle_{pp}$, mesons produced in minimum bias p+p interactions [14] are summarized in Table 2 and shown as a function of F in Figs. 3 and 4 together with the results for $\langle K_S^0\rangle_{pp}$.

The compilation is done starting from the threshold proton incident momentum for strangeness production ($p_{LAB} = 2.3$ GeV/c) up to about 400 GeV/c. This momentum range covers the momentum range of the existing nucleus–nucleus data. The presented data on neutral strange hadron production were obtained by bubble, streamer and time projection chamber experiments. High tracking precision in large fiducial volume is the characteristic feature of these detectors. It allows for an efficient measurement of neutral strange particle decays and their identification by testing the energy–momentum conservation law at the decay vertex for various decay hypothesis.

The measurement of charged kaon production is done using various experimental techniques. At low incident momenta (up to several GeV/c) the charged kaon yields were

extracted by exclusive analysis of hydrogen bubble chamber data (2.807, 3.67, 4.95, 5.52, 8 and 32 GeV/c [14]). At all incident momenta charged kaon production was measured by counter experiments, where the particle identification was done by Cherenkov (3.2, 3.7, 12.5, 19.2, 24 and 35–70 GeV/c [14]) and Time-of-Flight (3.349, 3.701, 4.133 GeV/c [14]) detectors or by both methods (ISR) [14]. In the case of counter experiments an interpolation between points at which differential cross sections were measured is necessary in order to get the yield of kaons in the full momentum space. This interpolation was done in the original papers for most of the results presented here.

Data on charged kaon production in full momentum space for p+p collisions at about 11-15 GeV/c (AGS-energies) are sparse. Therefore, we attempt to evaluate the mean multiplicities of charged kaons produced in minimum bias p+p collisions near 14.6 GeV/c from spectrometer measurements at fixed angles at 12.5 GeV/c and 19.2 GeV/c [14] which only partially cover the space spanned by rapidity and transverse momentum. Kaon yields had to be extrapolated to the regions not covered by measurements. The applied procedure consists of two steps. In the first step the measured transverse mass spectra were extrapolated to the full transverse mass domain in order to evaluate the rapidity density at various rapidities; the details of this procedure are described in [12]. In the second step the rapidity densities were interpolated and extrapolated to the low and high rapidity tails by a Gaussian fit. The integral of the fitted Gaussian in the limits from target rapidity to beam rapidity was used as an estimation of the mean multiplicity of the charged kaons. The error on the multiplicity was taken from the fit procedure and in addition an average systematic error stated by the various experiments has been added linearly to the statistical error. Multiplicity results obtained by others [17, 18] using similar extrapolation procedures are also given. Various experimental techniques give consistent results as seen in Table 2 and Figs. 3 and 4.

2.2 Construction of N+N Multiplicities

In the following sections we are going to discuss the strangeness production in central nucleus–nucleus collisions. Therefore in order to be able to carry out a meaningful study of the strangeness production dependence on the collision energy and nucleus mass number, A , we have to construct the results for nucleon–nucleon, N+N, interactions i.e. for nucleus–nucleus collisions at $A = 1$ [19]. These results are defined as a weighted average of the data for p+p, p+n and n+n interactions, where the weight factors are equal to the probabilities for finding a given pair of nucleons in the projectile and target nuclei.

Unfortunately the results on strange hadron production in p+n interactions are very poor [20] and data for n+n interactions do not exist. Therefore the construction of the results for N+N interactions has to be based on the p+p data.

Charge symmetry of the strong interaction leads to the following relations between strange particle multiplicities in proton–proton and neutron–neutron interactions at the same incident energy [19]:

$$\langle \Lambda \rangle_{pp} = \langle \Lambda \rangle_{nn}, \quad (2)$$

$$\langle \bar{\Lambda} \rangle_{pp} = \langle \bar{\Lambda} \rangle_{nn}, \quad (3)$$

$$\langle K^+ \rangle_{pp} = \langle K^0 \rangle_{nn}, \quad (4)$$

$$\langle K^- \rangle_{pp} = \langle \bar{K}^0 \rangle_{nn}, \quad (5)$$

$$\langle K^0 \rangle_{pp} = \langle K^+ \rangle_{nn}, \quad (6)$$

$$\langle \bar{K}^0 \rangle_{pp} = \langle K^- \rangle_{nn}. \quad (7)$$

From the relations for kaon yields (Eqs. 4–7) follow that the mean multiplicity of produced kaons and antikaons, $\langle K + \bar{K} \rangle$, is equal in p+p and n+n interactions.

The strange particle multiplicities in p+n interactions can not be derived from p+p results using charge symmetry [19]. Therefore, following the procedure presented in Ref. [19], we assume that:

$$\langle \Lambda \rangle_{pn} = 0.5 \cdot (\langle \Lambda \rangle_{pp} + \langle \Lambda \rangle_{nn}) = \langle \Lambda \rangle_{pp}, \quad (8)$$

$$\langle \bar{\Lambda} \rangle_{pn} = 0.5 \cdot (\langle \bar{\Lambda} \rangle_{pp} + \langle \bar{\Lambda} \rangle_{nn}) = \langle \bar{\Lambda} \rangle_{pp}, \quad (9)$$

$$\langle K + \bar{K} \rangle_{pn} = 0.5 \cdot (\langle K + \bar{K} \rangle_{pp} + \langle K + \bar{K} \rangle_{nn}) = \langle K + \bar{K} \rangle_{pp}. \quad (10)$$

The above relations are obeyed within the errors by the p+n data in the incident momentum range 10–29 GeV/c.

According to the definition of nucleon–nucleon interactions the mean multiplicity of the particle a in these interactions for nucleus–nucleus collisions of identical nuclei is given by:

$$\langle a \rangle_{NN} = \left(\frac{Z}{A} \right)^2 \cdot \langle a \rangle_{pp} + 2 \cdot \frac{Z}{A} \cdot \left(1 - \frac{Z}{A} \right) \cdot \langle a \rangle_{pn} + \left(1 - \frac{Z}{A} \right)^2 \cdot \langle a \rangle_{nn}, \quad (11)$$

where Z and A are the numbers of protons and nucleons in a nucleus, respectively. From Eqs. 2–11 follows that:

$$\langle \Lambda \rangle_{NN} = \langle \Lambda \rangle_{pp}, \quad (12)$$

$$\langle \bar{\Lambda} \rangle_{NN} = \langle \bar{\Lambda} \rangle_{pp}, \quad (13)$$

$$\langle K + \bar{K} \rangle_{NN} = \langle K + \bar{K} \rangle_{pp}, \quad (14)$$

independent of A and Z of the colliding systems.

The Eqs. 12–14 are used in the following sections to derive the strangeness yield in nucleon–nucleon interactions.

3 Central Nucleus–Nucleus Collisions

In this section we have compiled data on the mean multiplicity of strange hadrons produced in central nucleus–nucleus collisions at incident momenta of 4.5–200 A·GeV/c.

In the compilation and analysis we included the data on strangeness production from JINR Synchrophasotron (4.5 A·GeV/c), BNL AGS (11.6 and 14.6 A·GeV/c) and CERN SPS (200 A·GeV/c). The data on strange particle production below 4.5 A·GeV/c are not included as they are relatively sparse; we are not aware of simultaneous measurements of Λ hyperons and kaons in the same reaction.

All data on mean multiplicity of Λ , $\bar{\Lambda}$ hyperons, K_S^0 , K^+ and K^- mesons produced in central nucleus–nucleus collisions at energies larger than 4.5 A·GeV/c are presented in Table 3 [21]. In the table the corresponding data for p+p interactions at the same energy per nucleon as the corresponding nucleus–nucleus results are also given. If data on p+p interactions are not available or of poor quality at the respective incident proton momentum, the strange hadron multiplicities were calculated by a linear interpolation procedure.

The data on Λ and K_S^0 production in central carbon and oxygen collisions with various nuclear targets (C–Pb) at 4.5 A·GeV/c were obtained by the SKM–200 Collaboration at the Dubna Synchrophasotron [21]. The strange particle decays were detected by a 2m long streamer chamber. Central collisions (5–15% of the inelastic cross section) were defined as those without spectator nucleons of the projectile nucleus. Approximate symmetry of the C+C, C+Ne and O+Ne collisions allowed for a reliable correction of K_S^0 yields for large acceptance cuts in the target fragmentation region. The reliability of the correction is lower for asymmetric collisions and therefore we limit ourself to the analysis of C+C, C+Ne, O+Ne and C+Cu, C+Zr collisions. Due to low statistics the data on these collisions were averaged for the three light systems and for the two heavier. The data for the light systems are referred in this paper as ‘O+Ne’ because the data for O+Ne collisions dominate the averaged sample.

Charged kaon production in central Si+Al collisions (7% of the inelastic cross section) and central Au+Au collisions (4% of the inelastic cross section) has been measured by the experiments E802/E859 and E866 [21] at the AGS. These experiments published K^+ and K^- –meson rapidity distributions covering about 1 to 1.5 rapidity units near midrapidity. Experiment E810 measured the Λ and K_S^0 production in central Si+Si collisions (10% of the inelastic cross section) [21]. Here the measurements cover the rapidity region of $1.4 < y < 3.2$ for Λ hyperons and $2.0 < y < 3.5$ for kaons. Therefore for all measurements an extrapolation to the low and high rapidity tails was necessary in order to evaluate the mean multiplicity of strange hadrons in full momentum space. In the extrapolation procedure we assumed that the rapidity distributions can be parametrized by a Gaussian. The parameters of the function were fitted to the measured rapidity distributions. The integral of the fitted function in the limits from target rapidity to beam rapidity was used as an estimation of the mean multiplicity.

The data on mean multiplicities of Λ , $\bar{\Lambda}$ hyperons, K_S^0 , K^+ and K^- mesons at CERN SPS (200 A·GeV/c) were obtained by the NA35 Collaboration [21]. The data originate

mostly from the analysis of strange particle decays registered by the NA35 streamer chamber. Some data on charged kaon production were obtained using the NA35 time projection chamber. The central collisions (2–6% of the inelastic cross section) were defined as those with the total energy deposited in the projectile spectator region lower than a given limit. The large acceptance of the streamer chamber and runs with various configurations of magnetic field and target position allowed to obtain strange particle yields in full momentum range for central S+S and S+Ag collisions [21]. The NA36 experiment at CERN SPS also published data on absolute strange particle yields in central sulphur–nucleus collisions at 200 A·GeV/c [22]. Good agreement with the NA35 data was shown [22]. In the QM’95 proceedings significant disagreement with NA35 Λ -data was reported [23], but the results of the revised analysis for $\bar{\Lambda}$ and K_S^0 were not shown. Therefore the NA36 data were not included in the current compilation.

4 Strangeness Production in Nuclear Collisions

In this section we present the basic features of strangeness production in central nucleus–nucleus collisions at various energies, its dependence on the sizes of colliding nuclei and collision energy. The results are compared with the corresponding data for nucleon–nucleon interactions.

In order to quantify the total production of strangeness we follow a procedure described in Alber et al. [21] and use the E_S ratio defined as

$$E_S = \frac{\langle \Lambda \rangle + \langle K + \bar{K} \rangle}{\langle \pi \rangle}, \quad (15)$$

where $\langle \pi \rangle$ is the mean multiplicity of all pions produced. The sum of all kaons and Λ hyperons even for the highest energies discussed here contains more than 70% of the total number of strange quarks produced [16]. Since the $\bar{\Lambda}/\Lambda$ ratio is always smaller than $\simeq 20\%$, the contribution of strange antiquarks in $\bar{\Lambda}$ to E_S is less than 5%. The correction for the unmeasured strange particles (remaining main contributors are η meson and $\Sigma^{+/-}$ hyperons) is model–dependent and it was not applied here. Thus the sum $\langle \Lambda \rangle + \langle K + \bar{K} \rangle$ is assumed in this paper to be proportional to the total strangeness production, this assumption may lead to about 10% systematic biases when comparing production at different energies and/or for various systems. The total kaon multiplicity is calculated as:

$$\langle K + \bar{K} \rangle = \langle K^+ \rangle + \langle K^- \rangle + 2 \cdot \langle K_S^0 \rangle \quad (16)$$

or, if the data on charged or neutral kaons do not exist (see Table 3), using approximate charge symmetry of the systems as:

$$\langle K + \bar{K} \rangle = 4 \cdot \langle K_S^0 \rangle \quad (17)$$

or

$$\langle K + \bar{K} \rangle = 2 \cdot (\langle K^+ \rangle + \langle K^- \rangle). \quad (18)$$

In the case of central Au+Au collisions at 11.6 A·GeV/c only data on charged kaon multiplicities exist. Neglecting the small charge asymmetry of the Au+Au system and using strangeness conservation law we can estimate $\langle\Lambda\rangle$ by:

$$\langle\Lambda\rangle_{AuAu} = \frac{2}{1.6 \pm 0.1} \cdot (\langle K^+ \rangle + \langle K^- \rangle) = 24 \pm 4, \quad (19)$$

where the factor 1.6 is equal to the ratio of the total number of produced hyperons to the number of produced Λ hyperons established experimentally for p+p interactions at AGS energies [16]. The procedure was checked using Si+Al/Si data at 14.6 A·GeV/c.

In Table 4 we summarize the values of $\langle\Lambda\rangle + \langle K + \bar{K}\rangle$, $\langle\pi\rangle$, the mean number of participant nucleons, $\langle N_P \rangle$, and the E_S ratio for central nucleus–nucleus collisions and nucleon–nucleon interactions at the corresponding energy. The experimental definition of the number of participant nucleons used is as follows: the number of the participant nucleons is equal to the net baryon number of all particles in the final state outside the ‘Fermi spheres’ ($p < 300$ MeV/c) of the projectile and target nuclei. The description of experimental techniques used to measure $\langle N_P \rangle$ can be found in the original papers quoted in the Ref. [12]. The $\langle\pi\rangle$ values were calculated on the basis of (approximate) charge symmetry of all systems as

$$\langle\pi\rangle = 3 \cdot (\langle h^- \rangle - \langle K^- \rangle), \quad (20)$$

where $\langle h^- \rangle$ is the mean multiplicity of negatively charged mesons taken from our previous compilation [12]. The $\langle K^- \rangle$ values summarized in the Table 3 are used for nucleus–nucleus collisions (at 4.5 A·GeV/c we assume $\langle K^- \rangle = 0$). For nucleon–nucleon interactions the $\langle K^- \rangle_{pp}$ values are used (see Table 3) which may introduce a bias smaller than 1% [19]. For central Au+Au collisions at 11.6 A·GeV/c the recent pion multiplicity value from Videbaek et al. [21] was used with the error deduced by us to be about 10%. The $\langle N_P \rangle$ values are taken from the compilation [12].

The ratio of strangeness per participant nucleon number defined as

$$B_S = \frac{\langle\Lambda\rangle + \langle K + \bar{K}\rangle}{\langle N_P \rangle} \quad (21)$$

is shown in Fig. 5 for central nucleus–nucleus collisions and nucleon–nucleon interaction as a function of F . The ratio increases for both types of collisions, being on average a factor of about two larger for nucleus–nucleus collisions relative to nucleon–nucleon interactions.

The dependence of the E_S ratio (see Eq. 15) on the projectile nucleus mass number (in all analyzed reactions the projectile nucleus is smaller than the target one) at Dubna, AGS and SPS energies is shown in Figs. 6a–6c, respectively. Note that the AGS data at 11.6 A·GeV/c (Au+Au) and 14.6 A·GeV/c (Si+Al/Si) are plotted in the same figure. The E_S ratio is larger for central nucleus–nucleus collisions than for nucleon–nucleon interactions at the same energy. This is observed for all analyzed energies. The enhancement factor ranges from 1.7 for C+Cu/Zr collisions at 4.5 A·GeV/c and S+S collisions at 200 A·GeV/c to 4.5 for Au+Au collisions at 11.6 A·GeV/c. We do not observe any significant dependence of the E_S ratio on the target nucleus mass number at fixed projectile and collision

energy. This is consistent with the observed independence of the strangeness suppression factor [16], λ_S , of the target nucleus mass number for proton–nucleus interactions [24]. The E_S ratio for these interactions is close to the E_S ratio for N+N interactions (see e.g. Ref. [25]). It indicates strong projectile dependence, e.g. the ratio for p+S interactions is about two times lower than the ratio for S+S collisions at 200 A·GeV/c. The data at AGS energies suggest a possible saturation of the E_S ratio with the volume of the system for collisions of large enough nuclei. The increase from Si+Al/Si collisions to Au+Au collisions is about 40%, whereas the increase from nucleon–nucleon interactions to Si+Al/Si collisions is by a factor of about 3.

The energy dependence of the E_S ratio for nucleon–nucleon interactions and central nucleus–nucleus collisions is shown in Fig. 7a and 7b, respectively. The E_S ratio increases with the energy in a monotonic way for nucleon–nucleon interactions (see Fig. 7a). A qualitatively different behaviour is observed for central nucleus–nucleus collisions; the fast increase of the E_S ratio occurs between Dubna and AGS energies, but the E_S values at AGS and SPS energies are similar (see Fig. 7b).

5 Discussion

We will start the discussion with a possible interpretation of the presented results in terms of a commonly used approach of an equilibrated hadronic gas. In such an approach the freeze-out temperature is expected to be approximately independent of the collision energy (for high enough energies). This leads to the weak dependence of E_S on F as indicated by AGS and SPS data. The rapid increase of E_S between Dubna and AGS energies may be interpreted as due to an increase of the strangeness saturation level (towards equilibrium) and/or an increase of the freeze-out temperature (possible, providing that the early stage temperature is lower than the high energy limit of the freeze-out temperature). This interpretation encounters, however, several problems. The rapid increase of the pion multiplicity observed between AGS and SPS energies remains unexplained. A complete description of the hadronic yields at SPS energies seems to be not possible [27, 28]. The chemical freeze-out temperature derived from strangeness and baryonic components is significantly higher at SPS energies (≈ 200 MeV [28]) than at AGS energies (≈ 110 MeV [29]). Therefore, an interpretation of the energy dependence of pion and strangeness production in central A+A collisions in terms of an equilibrated hadron gas approach seems to be inappropriate.

A different scenario is presented in the following. The volume and the collision energy dependence of the entropy production in nuclear collisions was shown to be consistent with the predictions of the generalized Landau model [13, 30]. Within this approach the increase of the entropy production which is observed between AGS and SPS energies [12] was interpreted as due to increase of the number of degrees of freedom in the matter created at the early stage of high energy heavy ion collisions. These results motivate the attempt to interpret data on strangeness production (compiled in this paper) within a similar approach.

The presented interpretation is based on the assumption that for collisions of large enough nuclei the E_S ratio is proportional to the equilibrium strangeness to entropy ratio at temperature T which is an increasing function of the collision energy³.

From basic thermodynamics follows that for massive particles the equilibrium particle number to entropy ratio increases with the temperature of the matter. The ratio reaches its saturation value, equal to the corresponding ratio for massless particles, for $T \gg m$. Thus the increase and a subsequent saturation of the E_S ratio for A+A collisions with F may be interpreted as a reflection of the above described behaviour, providing that the strangeness carriers are massive. This interpretation, however, is inconsistent with the observed rapid increase of the entropy production occurring between AGS and SPS energies.

In the following a consistent interpretation is proposed. The rapid increase of the E_S ratio for A+A collisions with F observed at low energies is due to the mentioned above increase of the equilibrium strangeness to entropy ratio with T for massive strangeness carriers. This increase may continue above the AGS energy. The E_S ratio for N+N interactions and A+A collisions changes by a similar factor between Dubna and AGS energies. Thus the scaled⁴ E_S values for N+N interactions may be used for an approximate extrapolation of the E_S ratio for A+A collisions above AGS energies (see open squares and a solid line drawn to guide the eye in Fig. 8). The E_S increase with F can continue until the transition, e.g. from hadronic or constituent quark matter [31] to a Quark Gluon Plasma, occurs. As the equilibrium strangeness to entropy ratio is lower for Quark Gluon Plasma than for other forms of strongly interacting matter, the rapid decrease of the E_S ratio is expected in the transition region. Its hypothetical position is between AGS and SPS energies. The mass of the strangeness carriers is expected to be significantly lower in the Quark Gluon Plasma ($m_S \approx 150$ MeV) than in the hadronic or constituent quark matter ($m_S \approx 500$ MeV) due to approximate chiral symmetry restoration. Therefore the energy dependence of the E_S ratio above the transition region should be significantly weaker than below the transition⁵. The horizontal dashed line in Fig. 8 indicates the expected E_S dependence on F in the approximation of massless strange quarks ($m_S \ll T$).

6 Summary and Conclusions

We would like to summarize the paper as follows.

- The data on mean multiplicity of strange hadrons produced in central nucleus–nucleus collisions and minimum bias proton–proton interactions at incident momenta 2.8–400 A·GeV/c were compiled. This allowed the construction of the cor-

³In the generalized Landau model the early stage temperature is proportional to F (see Eq. 1) for $\sqrt{s} \gg 2 \cdot m_p$ [13].

⁴The scaling factor is equal to the ratio $E_S(Si + Al/Si)/E_S(N + N) = 2.8$ at 14.6 A·GeV/c.

⁵The quantitative results on the temperature dependence of the strangeness to entropy ratio obtained within simple models of hadronic matter and Quark Gluon Plasma can be found in Ref. [32].

responding results for nucleon–nucleon interactions which serve as a reference in studying properties of nucleus–nucleus collisions. The dependences of the ratios strangeness/pion and strangeness/baryon on the collision energy and the system size were presented and discussed. Strangeness enhancement is observed in central nucleus–nucleus collisions relative to nucleon–nucleon interactions at all studied energies. The ratio strangeness/pion shows qualitatively different behaviour as a function of collision energy for central nucleus–nucleus collisions and nucleon–nucleon interactions.

- Within a statistical approach the behaviour of the strangeness to pion ratio can be interpreted as due to a transition to a new form of matter (presumably Quark Gluon Plasma). This interpretation is consistent with the previous observation of the transition in the analysis of the entropy production.

We would like to conclude that experimental data on pion and strangeness production in central nucleus–nucleus collisions in the transition region are needed.

Acknowledgments

We would like to thank J.W. Harris, B. L. Friman, J. Knoll, St. Mrówczyński and H. Ströbele for numerous discussions and critical comments.

References

- [1] T. D. Lee, Quark Matter'95, Nucl. Phys. **A590** (1995) 11c.
- [2] J. C. Collins and M. J. Perry, Phys. Rev. Lett. **34** (1975) 151.
- [3] E. V. Shuryak, Phys. Rep. **C61** (1980) 71 and **C115** (1984) 151.
- [4] Proceedings of the Eleventh International Conference on Ultra-Relativistic Nucleus-Nucleus Collisions, Quark Matter'95, Monterey, California, USA, January 9-13, 1995, eds.: A. M. Poskanzer, J. W. Harris and L. S. Schroeder, Nucl. Phys. **A590** (1995).
- [5] T. Alber et al. (NA49 Collab.), Phys. Rev. Lett. **75** (1995) 3814.
- [6] F. Karsch and E. Laermann, Rep. Prog. Phys. **56** (1993) 1347,
F. Karsch, Quark Matter'95, Nucl. Phys. **A590** (1995) 367c.
- [7] P. Koch, B. Müller and J. Rafelski, Phys. Rep. **142** (1986) 321.
- [8] Y. Miake and G. S. F. Stephans et al., (E802 Collab.), Z. Phys. **C38** (1989) 135.
- [9] M. Gaździcki et al. (NA35 Collab.), Nucl. Phys. **A498** (1989) 375c.
- [10] T. Matsui and H. Satz, Phys. Lett. **178B** (1986) 416.
- [11] A. Bussiere et al., (NA38 Collab.) Z. Phys. **C38** (1988) 117.
- [12] M. Gaździcki and D. Röhrich, Z. Phys. **C65** (1995) 215.
- [13] M. Gaździcki, Z. Phys. **C66** (1995) 659.
- [14] **p+p data:**
 - 2.807 GeV/c: W. J. Fickinger et al., Phys. Rev. **125** (1962) 2082.
 - 3.2 and 3.7 GeV/c: J. T. Reed et al., Phys. Rev. **168** (1968) 1495.
 - 3.349, 3.701 and 4.133 GeV/c: W. J. Hogan, P. A. Piroue and J. S. Smith, Phys. Rev. **166** (1968) 1472.
 - 3.67 GeV/c: R. I. Louttit et al., Phys. Rev. **123** (1961) 1465.
 - 4.95 GeV/c: E. Bierman, A. P. Colleraine and U. Nauenberg, Phys. Rev. **147** (1966) 922.
 - 5.52 GeV/c: G. Alexander et al., Phys. Rev. **154** (1967) 1284.
 - 6 GeV/c: R. L. Eisnev et al., Nucl. Phys. **B123** (1977) 361.
 - 6.92 GeV/c: G. Alexander et al., Nuovo Cimento **53A** (1968) 455.
 - 7.87 GeV/c: M. Firebaugh et al., Phys. Rev. **172** (1968) 1354.
 - 8 GeV/c: G. Ascoli et al., *Proceedings of the Thirteenth International Conference on High-Energy Physics, Berkeley, 1966* (University of California Press, Berkeley, 1967), abstract 9.a.6.
 - 12 GeV/c: C. W. Akerlof et al., Phys. Rev. **D3** (1971) 645.

12, 24 GeV/c: V. Blobel et al., Nucl. Phys. **B69** (1974) 454.
 12, 24 GeV/c: M. Fesefeldt et al., Nucl. Phys. **B147** (1979) 317.
 12.4 GeV/c: K. Jaeger et al., Phys. Rev. **D11** (1975) 1756.
 19 GeV/c: P. Aahlin et al., Phys. Scripta **21** (1980) 12.
 19.2 GeV/c: J. V. Allaby et al., *CERN Report No. 70-12*, (1970) (unpublished).
 24 GeV/c: U. Amaldi et al., Nucl. Phys. **B86** (1975) 403.
 24.5 GeV/c: J. Bartke et al., Nuovo Cimento **29** (1963) 8.
 32 GeV/c: E. E. Zabrodin et al., Phys. Rev. **D52** (1995) 1316.
 69 GeV/c: V. V. Ammosov et al., Nucl. Phys. **B115** (1976) 269.
 100 GeV/c: M. Alston-Garnjost et al., Phys. Rev. Lett. **35** (1975) 142.
 102 GeV/c: J. W. Chapman et al., Phys. Lett. **47B** (1973) 465.
 147 GeV/c: D. Brick et al., Nucl. Phys. **B164** (1980) 1.
 200 GeV/c: J. Allday et al., Z. Phys. **C40** (1988) 29.
 205 GeV/c: K. Jaeger et al., Phys. Rev. **D11** (1975) 2405.
 300 GeV/c: F. LoPinto et al., Phys. Rev. **D22** (1980) 573.
 300 GeV/c: A. Sheng et al., Phys. Rev. **D7** (1975) 1733.
 360 GeV/c: M. Asai et al., Z. Phys. **C27** (1985) 11.
 400 GeV/c: R. D. Kass et al., Phys. Rev. **D20** (1979) 605.
 405 GeV/c: H. Kichimi et al., Phys. Rev. **D20** (1979) 37.
 289, 498 GeV/c: Cf. Ref. [17, 18].

[15] E. Fermi, Prog. Theor. Phys. **5** (1950) 570.

[16] A. K. Wróblewski, Acta Phys. Polonica, **B16** (1985) 379.

[17] M. Antinucci et al., Nuovo Cimento Letters **6** (1973) 121 and references therein.

[18] A.M. Rossi et al., Nucl. Phys. **B84** (1975) 269 and references therein.

[19] M. Gaździcki and O. Hansen, Nucl. Phys. **A528** (1991) 754.

[20] **p+n data:**

4–8 GeV/c: R. E. Ansorge et al., Phys. Rev. **D10** (1974) 32.

10–24 GeV/c: R. E. Ansorge et al., Nucl. Phys. **B103** (1976) 509.

11.6 GeV/c: D. Hochman et al., Nucl. Phys. **B89** (1975) 383.

[21] **A+A data:**

4.5 A·GeV/c: M. Anikina et al., (SKM–200 Collab.) Z. Phys. **C25** (1984) 1.

11.6, 14.6 A·GeV/c: F. Videbaek et al., (E866 Collab.) Nucl. Phys. **A590** (1995) 249c.

14.6 A·GeV/c: S.E. Eiseman et al. (E810 Collab.), Phys. Lett. **B297** (1992) 44.

14.6 A·GeV/c: T. Abbott et al. (E802 Collab.), Phys. Rev. **C50** (1994) 1024.

14.6 A·GeV/c: G. Stephans et al. (E802/E859 Collab.), Nucl. Phys. **A566** (1994) 269c.

200 A·GeV/c: T. Alber et al., (NA35 Collab.) Z. Phys. **C64** (1994) 195.

200 A·GeV/c: J. Bächler et al., (NA35 Collab.) Z. Phys. **C58** (1993) 367.

- [22] E. Andersen et al., (NA36 Collab.) Phys. Lett. **B316** (1993) 603.
- [23] E. G. Judd et al., (NA36 Collab.) Nucl. Phys. **A590** (1995) 291c.
- [24] H. Białkowska, M. Gaździcki, W. Retyk and E. Skrzypczak, Z. Phys. **C55** (1992) 491.
- [25] M. Gaździcki et al. (NA35 Collab.), Nucl. Phys. **A590** (1995) 197c.
- [26] J. Barrette et al. (E814 Collab.), Phys. Rev. **C50** (1994) 3047.
- [27] J. Cleymans, K. Redlich, H. Satz and E. Suhonen, Z. Phys. **C58** (1993) 347.
- [28] J. Sollfrank, M. Gaździcki, U. Heinz and J. Rafelski, Z. Phys. **C61** (1994) 659.
- [29] J. Cleymans, D. Elliott, H. Satz and R.L. Thews, CERN preprint, CERN-TH/95-298 (1995).
- [30] L. D. Landau, Izv. Akad. Nauk SSSR **78** (1953) 51.
- [31] O. D. Chernavskaya and E. L. Feinberg, Proceedings of A NATO Advanced Research Workshop on *Hot Hadronic Matter: Theory and Experiment*, held June 27–July 1, 1994, Divonne, France, eds.: J. Letessier, H. H. Gutbrod and J. Rafelski, NATO ASI Series B: Physics Vol. 346 (1995) 117.
- [32] J. Kapusta and A. Mekjan, Phys. Rev. **D33** (1986) 1304.

Table Captions

Table 1

The compiled results on the mean multiplicities of Λ , $\bar{\Lambda}$ hyperons and K_S^0 mesons, $\langle\Lambda\rangle_{pp}$, $\langle\bar{\Lambda}\rangle_{pp}$ and $\langle K_S^0\rangle_{pp}$, produced in minimum bias proton–proton interactions at different momenta of incident protons p_{LAB} .

Table 2

The compiled results on the mean multiplicities of charged kaons, $\langle K^+\rangle_{pp}$ and $\langle K^-\rangle_{pp}$, produced in minimum bias proton–proton interactions at different momenta of incident protons p_{LAB} . In some cases (*) the results of two different extrapolation procedures are given, the symbol denotes the values taken from Ref. [17].

Table 3

The compiled results on the mean multiplicities of strange particles produced in central nucleus–nucleus collisions at different momenta per incident nucleon p_{LAB} [$A \cdot \text{GeV}/c$]. The corresponding multiplicities for p+p interactions obtained by an interpolation procedure are also shown.

Table 4

The total mean multiplicities of strange particles, $\langle\Lambda\rangle+\langle K+\bar{K}\rangle$, pions, $\langle\pi\rangle$, participant nucleons, $\langle N_P\rangle$, and the E_S ratio for central nucleus–nucleus collisions and nucleon–nucleon interactions at corresponding incident momenta per nucleon p_{LAB} [$A \cdot \text{GeV}/c$].

Table 1

p_{LAB} [GeV/c]	$\langle \Lambda \rangle_{pp}$	$\langle \bar{\Lambda} \rangle_{pp}$	$\langle K_S^0 \rangle_{pp}$
2.807	0.00068 ± 0.00019	—	—
3.67	0.0033 ± 0.0006	—	0.00083 ± 0.00018
4.95	0.0073 ± 0.0003	—	0.0019 ± 0.0003
5.52	0.0127 ± 0.0011	—	0.00364 ± 0.00010
6	0.0109 ± 0.0007	—	0.0034 ± 0.0003
6.92	0.0172 ± 0.0010	—	0.0064 ± 0.0005
7.87	0.0201 ± 0.0010	—	0.0072 ± 0.0006
12	0.0388 ± 0.0006	$0.00010^{+0.00003}_{-0.00006}$	0.0202 ± 0.0004
12.4	0.035 ± 0.004	—	0.023 ± 0.003
19	0.061 ± 0.002	—	0.0415 ± 0.0013
24	0.0657 ± 0.0008	$0.0007^{+0.0001}_{-0.0003}$	0.0495 ± 0.0006
24.5	0.037 ± 0.007	—	0.045 ± 0.004
69	0.109 ± 0.006	0.005 ± 0.001	0.109 ± 0.007
100	0.112 ± 0.013	0.008 ± 0.002	0.122 ± 0.010
102	0.099 ± 0.012	0.005 ± 0.002	0.141 ± 0.014
147	0.133 ± 0.006	0.025 ± 0.006	0.158 ± 0.006
200	0.08 ± 0.02	0.02 ± 0.01	0.16 ± 0.02
205	0.103 ± 0.011	0.012 ± 0.004	0.181 ± 0.014
300	0.111 ± 0.015	0.020 ± 0.004	0.21 ± 0.03
300	0.11 ± 0.01	0.031 ± 0.009	0.224 ± 0.018
360	0.12 ± 0.02	0.013 ± 0.004	0.26 ± 0.01
400	0.12 ± 0.01	0.013 ± 0.003	0.20 ± 0.02
405	0.125 ± 0.008	0.020 ± 0.004	0.232 ± 0.011

Table 2

p_{LAB} [GeV/c]	$\langle K^+ \rangle_{pp}$	$\langle K^- \rangle_{pp}$
2.807	0.00068 ± 0.00019	–
3.2	0.0019 ± 0.0003 *	–
3.2	0.0026 ± 0.0007	–
3.349	0.0022 ± 0.0004	–
3.67	0.0046 ± 0.0007	–
3.7	0.0033 ± 0.0005 *	–
3.7	0.0046 ± 0.0011	–
3.701	0.0044 ± 0.0008	–
4.133	0.0057 ± 0.0010	–
4.95	0.0069 ± 0.0010	–
5.52	0.0080 ± 0.0017	–
8	0.020 ± 0.004	–
12.5	0.07 ± 0.03	0.010 ± 0.004
12.5	–	0.008 ± 0.001 *
14.3	0.054 ± 0.008	–
19.2	0.107 ± 0.016	0.036 ± 0.005
24	0.102 ± 0.01	0.027 ± 0.003
24	0.13 ± 0.02 *	0.033 ± 0.005 *
32	–	0.05 ± 0.015
35	–	0.07 ± 0.02
43	–	0.08 ± 0.02
52	–	0.11 ± 0.03
70	0.21 ± 0.06	0.13 ± 0.03
289	0.337 ± 0.051	0.209 ± 0.031
498	0.367 ± 0.055	0.244 ± 0.037

Table 3

p_{LAB}	Reaction	$\langle\Lambda\rangle$	$\langle\bar{\Lambda}\rangle$	$\langle K_S^0\rangle$	$\langle K^+\rangle$	$\langle K^-\rangle$
4.5	p+p	0.006 ± 0.001	–	0.0019 ± 0.0004	0.006 ± 0.001	0
4.5	‘O+Ne’	0.091 ± 0.017	≤ 0.001	0.035 ± 0.014	–	–
4.5	C+Cu/Zr	0.112 ± 0.018	≤ 0.001	0.048 ± 0.016	–	–
11.6	p+p	0.038 ± 0.001	$(0.9\pm 0.6)10^{-4}$	0.019 ± 0.002	0.051 ± 0.017	0.010 ± 0.005
11.6	Au+Au	–	–	–	24 ± 2	5.0 ± 0.4
14.6	p+p	0.047 ± 0.002	$(2.1\pm 1.5)10^{-4}$	0.027 ± 0.003	0.065 ± 0.017	0.015 ± 0.007
14.6	Si+Al/Si	2.4 ± 0.2	–	1.47 ± 0.06	2.6 ± 0.3	0.66 ± 0.08
200	p+p	0.096 ± 0.01	0.013 ± 0.005	0.17 ± 0.01	0.28 ± 0.06	0.18 ± 0.05
200	S+S	9.4 ± 1.0	2.2 ± 0.4	10.5 ± 1.7	12.5 ± 0.4	6.9 ± 0.4
200	S+Ag	15.2 ± 1.2	2.6 ± 0.3	15.5 ± 1.5	17.4 ± 1.0	9.6 ± 1.0

Table 4

p_{LAB}	Reaction	$\langle \Lambda \rangle + \langle K + \bar{K} \rangle$	$\langle \pi \rangle$	$\langle N_P \rangle$	E_S
4.5	N+N	0.0158 ± 0.0015	1.87 ± 0.08	2	0.0084 ± 0.0009
4.5	'O+Ne'	0.23 ± 0.06	13.2 ± 0.6	19 ± 2	0.017 ± 0.005
4.5	C+Cu/Zr	0.30 ± 0.07	21.6 ± 0.9	–	0.014 ± 0.003
11.6	N+N	0.137 ± 0.018	3.12 ± 0.08	2	0.044 ± 0.006
11.6	Au+Au	82 ± 6	420 ± 50	355 ± 7	0.20 ± 0.03
14.6	N+N	0.181 ± 0.19	3.44 ± 0.08	2	0.053 ± 0.006
14.6	Si+Al/Si	8.6 ± 0.4	58 ± 6	42 ± 4	0.148 ± 0.017
200	N+N	0.896 ± 0.08	9.15 ± 0.08	2	0.098 ± 0.009
200	S+S	50 ± 4	273 ± 10	51.2 ± 5	0.183 ± 0.016
200	S+Ag	77 ± 6	474 ± 30	90 ± 10	0.162 ± 0.016

Figure Captions

Fig. 1.

Dependence of the mean multiplicity of Λ hyperons, $\langle\Lambda\rangle_{pp}$, produced in minimum bias proton–proton interactions on the Fermi variable F (see Eq. 1).

Fig. 2.

Dependence of the mean multiplicity of $\bar{\Lambda}$ hyperons, $\langle\bar{\Lambda}\rangle_{pp}$, produced in minimum bias proton–proton interactions on the Fermi variable F (see Eq. 1).

Fig. 3.

Dependence of the mean multiplicity of K_S^0 mesons, $\langle K_S^0\rangle_{pp}$ (circles), K^+ mesons, $\langle K^+\rangle_{pp}$ (squares), and K^- mesons, $\langle K^-\rangle_{pp}$ (triangles), produced in minimum bias proton–proton interactions on the Fermi variable F (see Eq. 1).

Fig. 4.

Dependence of the mean multiplicity of K_S^0 (circles), K^+ (squares) and K^- (triangles) mesons produced in minimum bias proton–proton interactions near the threshold on the Fermi variable F (see Eq. 1).

Fig. 5.

Dependence of the B_S ratio (see Eq. 21) on the Fermi variable F (see Eq. 1) for nucleon–nucleon interactions (squares) and central nucleus–nucleus collisions (circles).

Fig. 6.

Dependence of the E_S ratio (see Eq. 15) on the projectile nucleus mass number, A_P , at 4.5 A·GeV/c (a), 11.6 and 14.6 A·GeV/c (b) and 200 A·GeV/c (c). Two nucleon–nucleon points in Fig. (b) correspond to 11.6 and 14.6 A·GeV/c.

Fig. 7.

Dependence of the E_S ratio (see Eq. 15) on the Fermi variable F (see Eq. 1) for nucleon–nucleon interactions (a) and central nucleus–nucleus collisions (b).

Fig. 8.

Dependence of the E_S ratio (see Eq. 15) on the Fermi variable F (see Eq. 1) for scaled (see text) nucleon–nucleon interactions (open squares) and central nucleus–nucleus collisions (circles). See text for explanation of the lines.

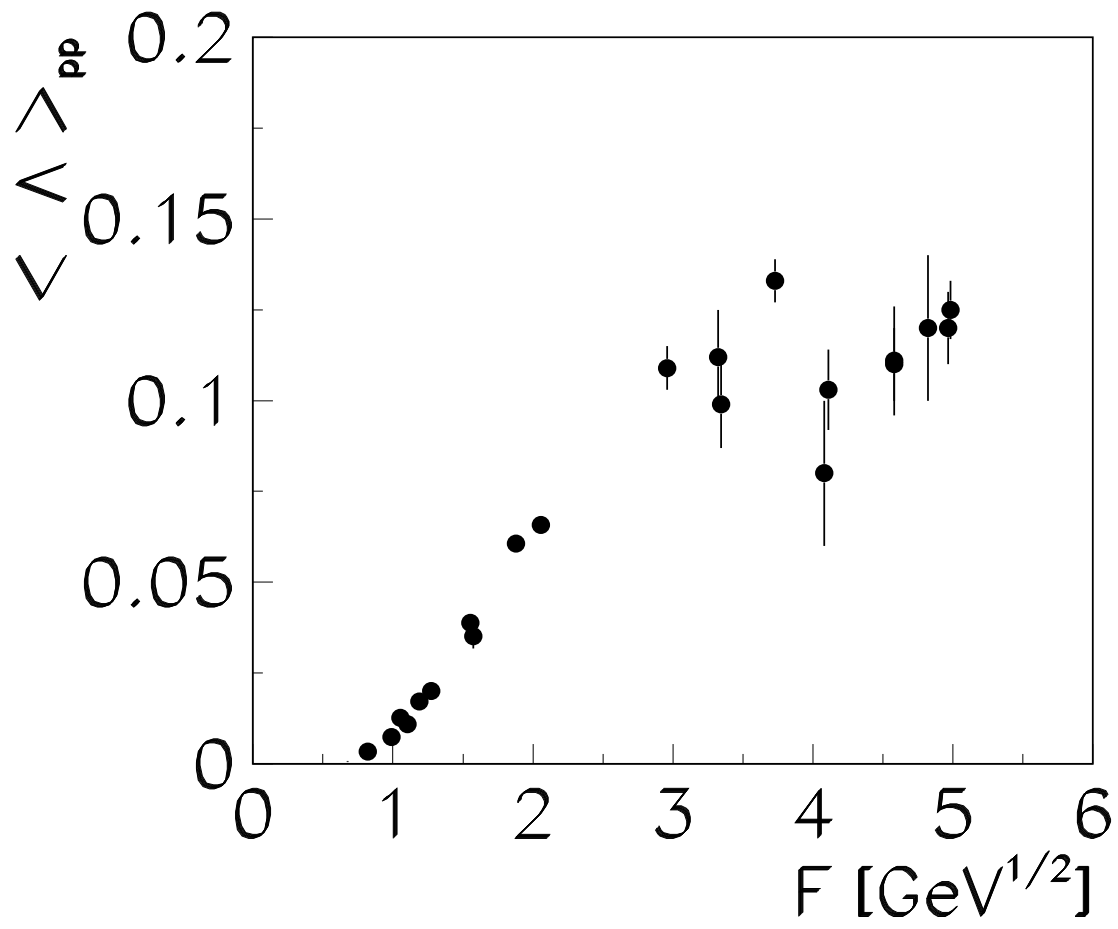


Figure 1:

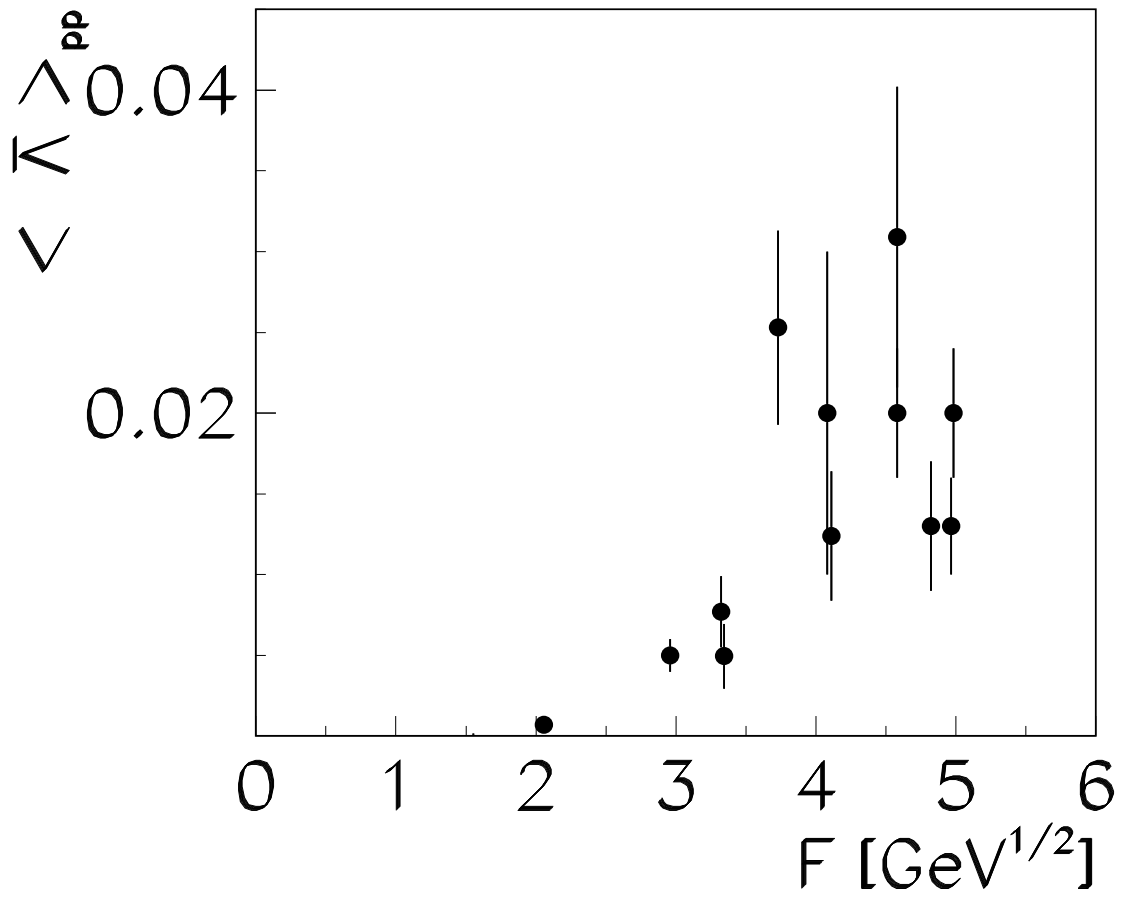


Figure 2:

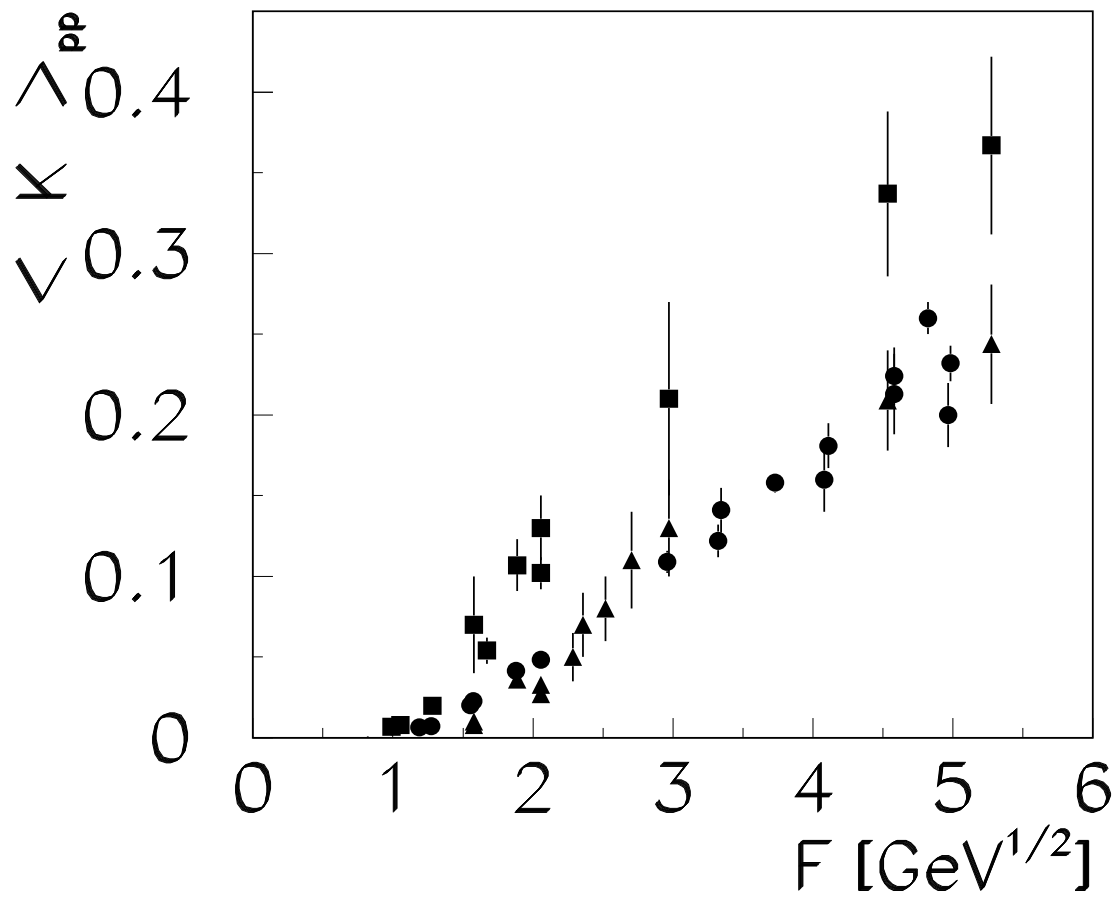


Figure 3:

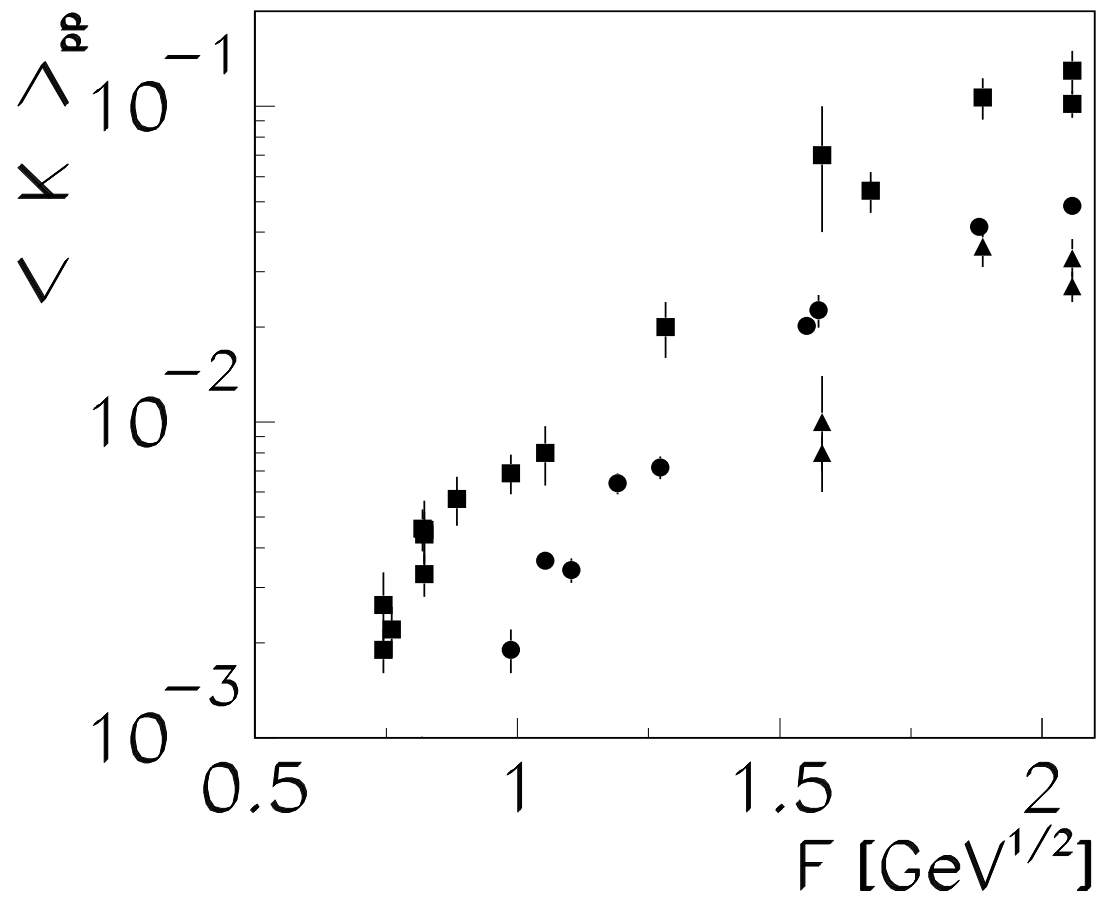


Figure 4:

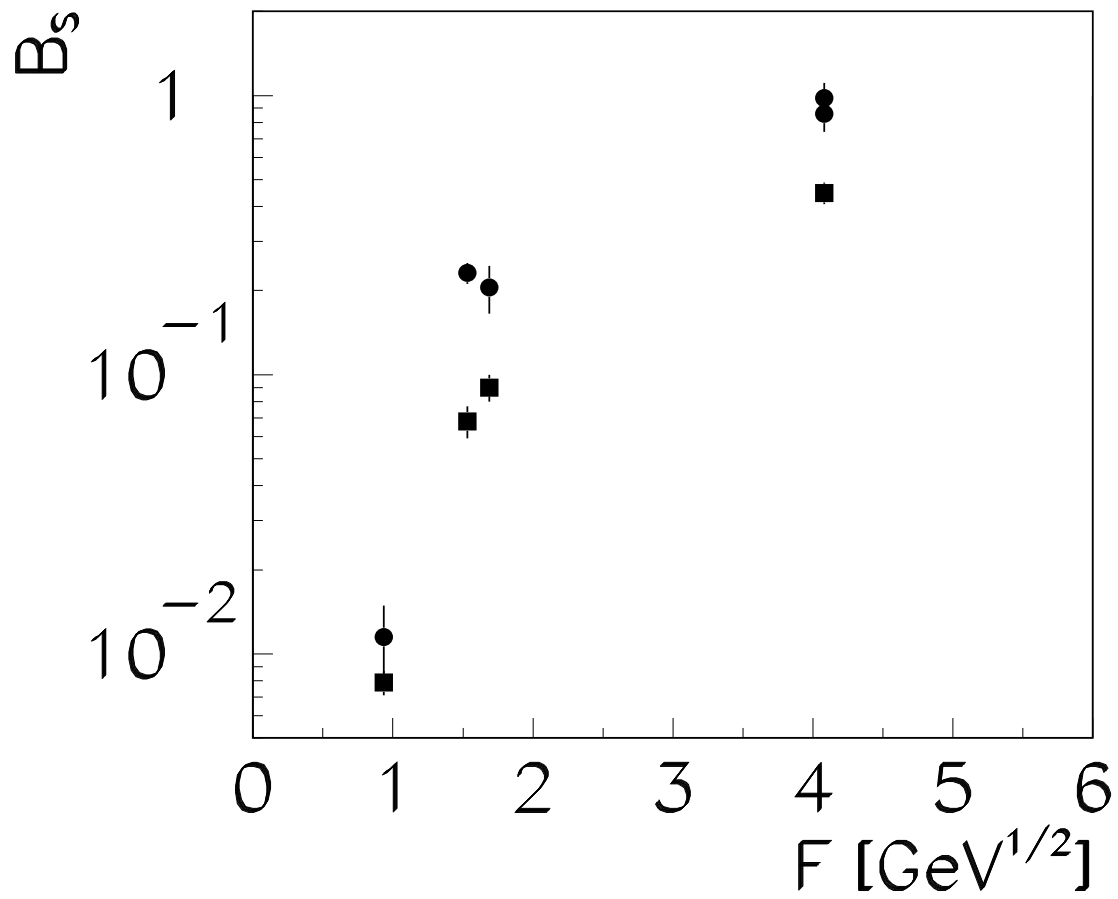


Figure 5:

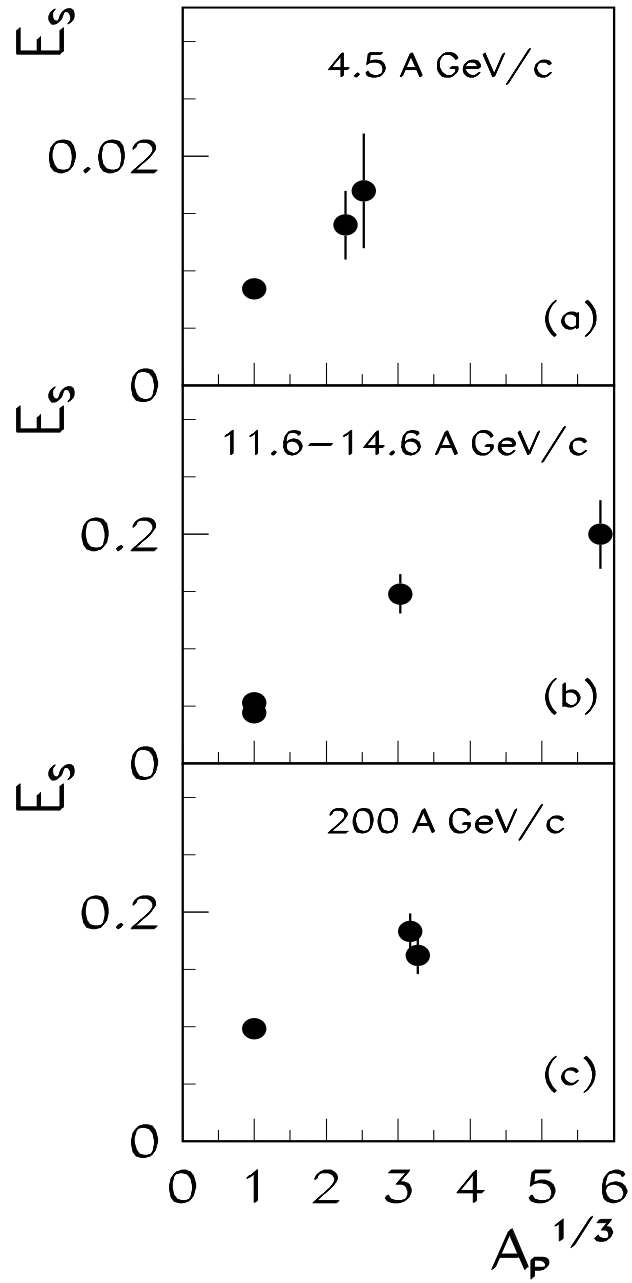


Figure 6:

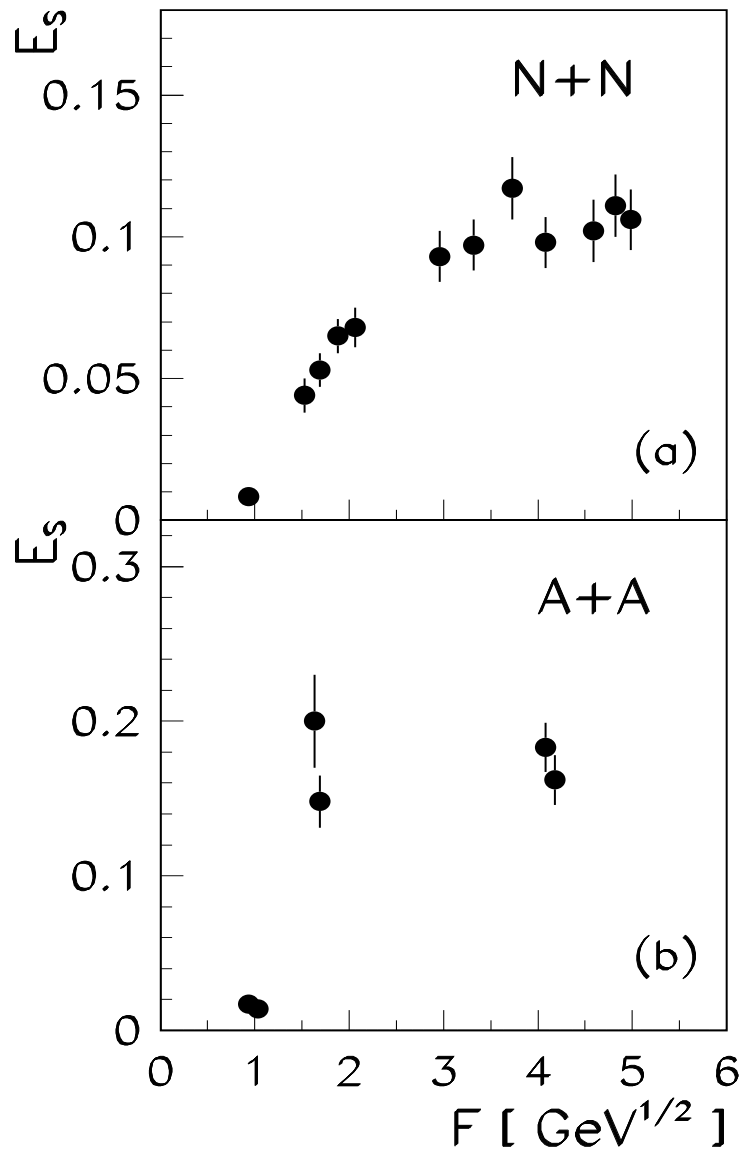


Figure 7:

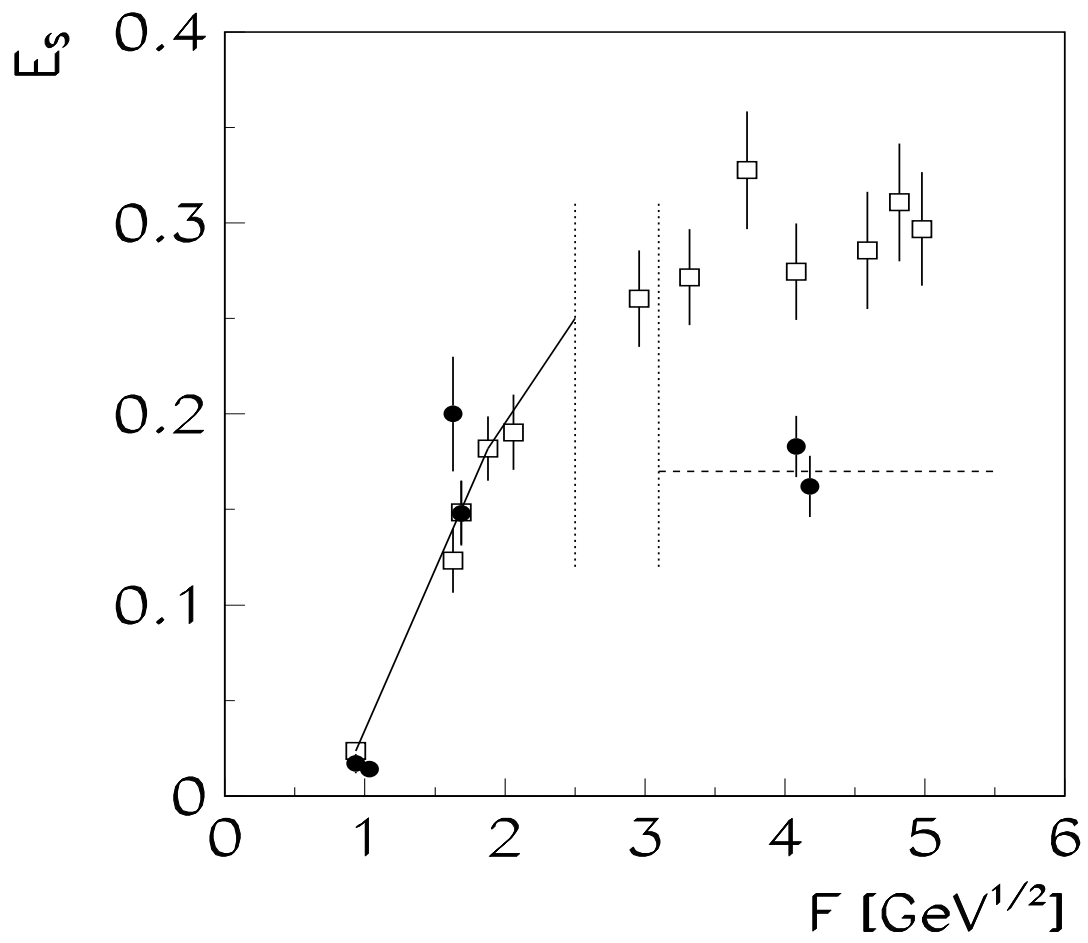


Figure 8: